Simulation of growth of Cu on Ag(001) at experimental deposition rates

J. A. Sprague
Materials Science and Technology Division, Naval Research Laboratory, Washington, DC 20375

F. Montalenti
INFM, Dipartimento di Scienza dei Materiali, Università di Milano-Bicocca, Via Cozzi 53, 20125 Milano, Italy
and Theoretical Division, Los Alamos National Laboratory, Los Alamos, New Mexico 87545

B. P. Uberuaga, J. D. Kress, and A. F. Voter
Theoretical Division, Los Alamos National Laboratory, Los Alamos, New Mexico 87545
(Received 8 October 2002; published 27 November 2002)

The initial stages of growth of (001)Cu films on (001)Ag substrates have been investigated using the temperature-accelerated dynamics (TAD) simulation method. The acceleration provided by TAD made it possible to simulate the deposition of Cu on (001)Ag at 77 K using a deposition rate of 0.04 ML/s, which matched previously reported experiments. This simulation was achieved without *a priori* knowledge of the significant atomic processes. The results showed that the increased in-plane lattice parameter of the pseudomorphic Cu reduces the activation energy for the exchange mode of surface diffusion, allowing short-range terrace diffusion and the formation of compact Cu islands on the second film layer at 77 K. Some unexpected complex surface diffusion processes and off-lattice atomic configurations were also observed.

DOI: 10.1103/PhysRevB.66.205415 PACS number(s): 68.55.Ac, 68.55.Jk

I. INTRODUCTION

Molecular-dynamics (MD) simulations can provide valuable insight into some of the atomic-level phenomena that control many material processes, including radiation damage, deformation, and vapor deposition. For an MD integration algorithm to remain stable, however, time steps must be no longer than several femtoseconds. For reasonable system sizes and current computational capacity, this limits total simulated times to several nanoseconds or less. For this reason, most MD investigations of thin-film deposition processes have employed effective deposition rates on the order of 10^9 ML/s, which are factors-of-10^8–10^{11} higher than experimental deposition rates. One possible result of such a high deposition rate is the effect of the energy introduced by one deposited atom on the response of the following deposited atom. This effect can be eliminated effectively by the careful choice of thermostat and deposition rate.[1] Such simulations can reveal details of phenomena occurring during and immediately following atom depositions, such as transient atom mobility,[2] downward funneling,[3] steering,[4] and athermal interface mixing.[5] However, thermally activated atomic processes with rates as low as one per second can have significant effects on thin-film microstructures. The high atom deposition rate required for conventional MD simulations cannot realistically model such processes. Therefore, the effects of phenomena such as terrace diffusion and interlayer transport on vapor-deposited crystal growth are excluded from the conventional MD simulations.

One approach to this dilemma is to create a catalog of the activation energies and kinetic prefactors for all significant thermal processes and to use this catalog in a kinetic Monte Carlo (KMC) simulation of the system of interest.[6,7] This approach allows the modeling of relatively large systems at realistic growth conditions for long times. Furthermore, features of the simulated structures can be directly compared to experimental measurements. A difficulty of the KMC method, however, is that it requires *a priori* knowledge of all significant atomic processes. This problem is especially severe for mechanisms with near-threshold activation energies at the temperature of interest. In this case, local variations in atomic environments can produce large variations in reaction rates.

An alternative approach to simulating processes over time scales of several seconds is provided by the temperature-accelerated dynamics (TAD) method,[8] one of several recently developed accelerated dynamics simulation techniques.[9] As briefly described in the following section, TAD uses a combination of molecular dynamics and statistical mechanics to correctly follow the actual dynamics of a system while providing accelerations of up to 10^9 in the calculations. This is achieved without any *a priori* knowledge of the relevant atomic processes. With an appropriate selection of conditions, this technique can allow the simulation of early stages of film growth at experimental deposition rates.[10,11]

The present investigation was motivated by the experiments of Egelhoff, Jr. and Jacob.[12] These authors reported persistent reflection high-energy electron-diffraction (RHEED) oscillations for several film/substrate systems at 77 K, a temperature at which they did not expect significant thermally activated surface diffusion. They interpreted the RHEED oscillations as indicative of quasi-layer-by-layer growth, which they attributed to terrace diffusion induced by the condensation energy of deposited atoms. Evans and co-workers[3,13] and later Yang, Wang, and Lu[14] demonstrated that this condensation energy effect does not exist, and proposed that the observed smoothness of the growing films was simply due to downward funneling. Here we show that in strained heteroepitaxial systems such as Cu deposited on (001)Ag significant terrace diffusion does take place at tem-

peratures as low as 77 K. The effect is not because of the condensation energy but is due to lowering of the exchange barrier for surface diffusion in second and higher film layers by the biaxial tensile strain in the film.

II. SIMULATION DETAILS

A. The TAD method

Because the TAD method has been described in detail by Sørensen and Voter,[8] only a brief discussion of its details will be given here. The basis of this method is the well-known fact that the rate at which any thermally activated process occurs can be increased by simply increasing the temperature of the system under study. For a harmonic system, this temperature dependence is given by the Arrhenius relation

$$\text{rate} = \nu_0 * \exp\left(-\frac{E_A}{kT}\right), \tag{1}$$

where ν_0 is the rate prefactor, E_A is the activation barrier energy, k is Boltzmann's constant, and T is the absolute temperature. This effect has been applied to accelerate activated processes in conventional MD simulations by computationally annealing the system. As applied to film deposition,[15] a few atoms are deposited at low temperature, the system temperature is raised to increase the rate of activated processes, the system is cooled back down to low temperature, and the process is repeated until the desired amount of material has been added. Equation (1) shows, however, that a temperature increase will not preserve the relative rates of processes with different activation barriers. Thus, unless only one activation barrier is significant, a simple temperature increase will not correctly preserve the system dynamics at the base temperature.

The TAD method addresses this problem by assuming that the system follows first-order kinetics, and that the harmonic approximation[16] to transition state theory[17–19] (TST) applies to the system under study. TST implies that for any transition between two states of the system, a dividing surface in configuration space can be defined such that a reactive transition occurs any time a system trajectory crosses this surface. This implies that there are no correlations between successive transitions. First-order kinetics and the harmonic approximation allow us to relate the time at which a transition is observed at an elevated temperature to the time at which it would have occurred at a lower temperature by a simple equation:

$$t_{i,\text{low}} = t_{i,\text{high}} \exp\left[\frac{E_{A,i}}{k}\left(\frac{1}{T_{\text{low}}} - \frac{1}{T_{\text{high}}}\right)\right], \tag{2}$$

where $E_{A,i}$ is the activation barrier (energy at the saddle point minus energy at the minimum) of transition i, and T_{low} and T_{high} are the system temperature and elevated temperature, respectively. The method is implemented by first performing a ''basin-constrained'' simulation at an increased temperature. In this simulation, MD is performed at the elevated temperature until a transition is detected. The minimum-energy path for the transition is then determined by the nudged-elastic-band method,[20,21] thus defining the activation barrier. Equation (2) then defines the extrapolated time for that transition to occur at T_{low}. The simulation is continued in the original basin, and additional transitions are detected and analyzed. To determine when sufficient information has been collected to define the transition with the shortest waiting time at T_{low}, we further assume that all possible transitions in the system have prefactors greater than $\nu_{\min}$. This leads to the result that the basin-constrained MD must be continued at T_{high} for a time $t_{\text{high,stop}}$:

$$t_{\text{high,stop}} = \frac{\ln(1/\delta)}{\nu_{\min}} \left\{ \frac{\nu_{\min} t_{\text{low,short}}}{\ln(1/\delta)} \right\}^{T_{\text{low}}/T_{\text{high}}}, \tag{3}$$

where $t_{\text{low,short}}$ is the observed transition with the shortest waiting time at T_{low}, and δ is the (low) probability that there is a yet unseen transition with a shorter waiting time at T_{low}. At this point, the first low-temperature transition is accepted, and the basin-constrained MD is begun again in the new state.

As noted previously,[8] the TAD algorithm can be slowed down considerably whenever there is a sequence of cyclical low-barrier transitions that occurs many times (perhaps millions) during the evolution of the system. From Eq. (2), the computational boost depends exponentially on the activation barrier, so that the overhead of analyzing each low-barrier transition can easily overcome all of the advantages of the TAD method. In an extensions of TAD, once a given transition has been seen a sufficient number of times to define its statistical distribution of waiting times, KMC is used to predict a set of transition times that are applied to the state (the transition is ''synthesized'') until the next regular transition is accepted. As will be discussed later, this extension was critical for the present investigation, since a number of very low-barrier transitions occurred in this system.

To implement the TAD method for the growth of Cu on (001)Ag, a substrate was created comprising seven 98-atom Ag layers, the bottom three of which were fixed. Boundary conditions were periodic in the *x-y* plane, with free surfaces in the *z* direction. The bottom active layer was thermostatted at 77 K using Langevin dynamics. As detailed in the following section, embedded-atom method (EAM) potentials[22] were used to model Ag-Ag, Cu-Cu, and Ag-Cu interactions. The simulation sequence was begun with a conventional MD simulation of Cu atom deposition at a random position in the *x-y* plane for an incident energy of 0.1 eV. Following 2 ps of this MD simulation, the system was evolved by TAD. The times between Cu atom depositions were chosen to duplicate the statistics of thermal evaporation with an average rate of 0.04 ML/s (0.245 s per atom). The sequence was then repeated for a total of 147 deposited atoms (1.5 ML). Atomic configurations were saved for each accepted configuration, as well as the saddle points and final configurations for each observed high-temperature transition. A file was also recorded containing activation barriers and waiting times for each accepted transition. The total actual simulated time was 45.7 s, with a minimum time between deposited atoms of 1.95 ms and a maximum of 1.86 s. To aid the analysis of the TAD results, a conventional MD simulation of Cu deposition on (001)Ag was performed for a system temperature of 77 K

using the same initial positions of the depositing atoms, but with only 2 ps between deposition events.

B. The Cu-Ag interatomic potential

The copper and silver interactions were described using an EAM (Ref. 22) interatomic potential, in which the energy of an atom i is given by

$$E_i = \frac{1}{2}\sum_j \phi_{t_i t_j}(r_{ij}) + F\left[\sum_j \rho_{t_j}(r_{ij})\right], \tag{4}$$

where r_{ij} is the scalar distance between atoms i and j, $\phi(r)$ is the pair potential, $\rho(r)$ is the density function, F is the embedding function, and t_i indicates the type of atom i (A or B for an A-B system). The nonlinearity of F gives the EAM potential its many-body nature. For each of the pure elements, the Voter-Chen[23] form was employed, in which the lattice constant (a_0), cohesive energy (E_{coh}), and bulk modulus (B) are reproduced exactly, while five parameters (three describing the Morse pair potential, one for the exponent of the density function, and one for the cutoff distance) are optimized to give the best fit to the vacancy formation energy, cubic elastic constants, and gas-phase diatomic bond length and bond energy. The details of the fitting procedure can be found in two references by Voter.[24,25] The optimized parameters, which have been given previously for both Cu (Ref. 26) and Ag,[27] are included here for completeness: For copper, $a_0 = 3.615$ Å, $E_{\mathrm{coh}} = 3.54$ eV, and $B = 1.419 \times 10^{12}$ erg/cm^3, $D_M = 0.7366$ eV, $R_M = 2.325$ Å, and $\alpha_M = 1.919$, $\beta_M = 4.043$, and $r_{\mathrm{cut}} = 4.961$ Å. For silver, $a_0 = 4.09$ Å, $E_{\mathrm{coh}} = 2.85$ eV, and $B = 1.036 \times 10^{12}$ erg/cm^3, $D_M = 0.6721$ eV, $R_M = 2.570$ Å, and $\alpha_M = 1.826$, $\beta_M = 3.906$ Å^{-1}, and $r_{\mathrm{cut}} = 5.542$ Å.

For the Cu-Ag interaction, we employed the form suggested by Johnson,[28] in which the cross pair potential is defined in terms of the pair potentials and density functions from the pure elements,

$$\phi_{AB}(r) = \frac{1}{2}\left[\frac{\rho_B(r)}{\rho_A(r)}\phi_{AA}(r) + \frac{\rho_A(r)}{\rho_B(r)}\phi_{BB}(r)\right] \tag{5}$$

[to prevent taking a ratio of infinitesimal quantities near the cutoff distance, a small value (0.0002) was added to each of the ρ denominators]. A pure-element EAM potential is invariant under a transformation in which a linear term is added to the embedding function and a compensating amount of $\rho(r)$ is subtracted from $\phi(r)$. However, this transformation does in general change the properties of an EAM alloy potential involving that element. Johnson showed that if the cross potential is defined by Eq. (5), then the alloy is also invariant under this type of transformation of the component elements. Although there is no physical justification for restricting the alloy potential in this way, the use of Eq. (5) offers an appealingly simple path for constructing the alloy potential. Once the pure-element functions have been specified, only a single degree of freedom remains: the relative scaling of the two density functions $\rho_A(r)$ and $\rho_B(r)$.[24] To pin down this parameter, we followed the suggestion of Foiles, Baskes, and Daw,[29] that the most important quantities to fit for an alloy are the two heats of solution at infinite dilution. Varying s_{Ag}, the relative scaling of $\rho_{\mathrm{Ag}}(r)$, a value of $s_{\mathrm{Ag}} = 1.253$ gave both heats of solution (0.41 eV for Ag in Cu and 0.23 eV for Cu in Ag) in excellent agreement with experiment[29] (0.39 eV for Ag in Cu and 0.25 eV for Cu in Ag). Interestingly, this optimal value for s_{Ag} is very close to the ideal value of 1.29 for which the ρ sum in the perfect Cu and Ag crystals is matched (using $s_{\mathrm{Ag}} = 1.29$ would change the predicted heats of solution by less than 0.05 eV). This is not typical of our experience with other cross potentials.

C. Reliability of the potentials

The results of the TAD simulations presented in this paper were obtained with embedded-atom method interatomic potentials. We have reason to believe that our potentials do give a good description of the real system, Cu/Ag(001). First, we note that the single-adatom diffusion barriers for the pure systems Ag/Ag(001) and Cu/Cu(001) obtained with these potentials[30] are in very good agreement with *ab initio* calculations.[31,32] (The hop barriers are within 0.05 eV and exchange barriers are too low by 0.1–0.15 eV. For a comprehensive comparison between semiempirical, *ab initio*, and experimental barriers on fcc metal surfaces, see Montalenti and Ferrando).[33] This is an important check because no surface data was included in the fitting procedure for the potentials.

Concerning the Ag-Cu interaction, we have noted above that, although only a single parameter was adjusted in fitting the cross potential, the experimental heats of solutions for both Ag in Cu and Cu in Ag are correctly reproduced by the potentials. In order to check the reliability of the alloy potential in describing surface dynamics, we compared the diffusion barriers for the jump and the exchange mechanism for a single Cu adatom on a Ag(001) surface with *ab initio* calculations. We did this using density-functional theory (DFT) as implemented in the VASP code.[34] Ultrasoft pseudopotentials[35] were used to represent the core electrons, and the valence electronic wave functions were expanded in plane waves. The simulation cell consisted of four layers (plus the adatom), with each layer containing 18 atoms. The bottom layer was kept fixed.

We started by performing Γ-point ($1\times1\times1$ k-point sampling of the Brillouin zone) calculations, using the Perdew-Wang 1991 (PW91) exchange-correlation functional[36] and a plane-wave energy cutoff of 234 eV. The activation energy for the hop of a single Cu adatom on Ag(001) was calculated to be $E_j^{\mathrm{VASP}} = 0.63$ eV. With our potentials, we found $E_j^{\mathrm{EAM}} = 0.62$ eV. Increasing the k-point sampling did not appreciably change the results. Indeed, using a $2\times2\times1$ mesh ($k_x \times k_y \times k_z$, where the z direction is perpendicular to the surface), we still found $E_j^{\mathrm{VASP}} = 0.63$ eV. We conclude that the jump barrier for Cu on Ag(001) calculated with our potentials is in excellent agreement with the *ab initio* results.

As a final check, we looked at the exchange process for an isolated Cu adatom on the Ag(001) surface. The saddle-point configuration was found using the nudged-elastic-band method, including its most recent developments, especially the climbing image algorithm.[21,37] A Γ-point calculation

yielded $E_{ex}^{VASP}=0.38$ eV; increasing the *k*-point sampling did not change the result, giving $E_{ex}^{VASP}=0.38$ eV,[38] for a $2\times2\times1$ mesh. In this case, the agreement between *ab initio* and EAM results was not as satisfactory, with $E_{ex}^{EAM}=0.52$ eV. This discrepancy might be an indication of a limitation of the potential to accurately describe Cu/Ag(001). However, it is also possible that the PW91 functional is not accurate for this case.

We also tested the agreement between the EAM and DFT for some larger Cu configurations on Ag(001) (for example, small Cu islands on Ag). We found that when the calculations were not sufficiently converged (such as when too few *k* points or too few layers in the slab were used), DFT preferred to make more compact structures, with Cu atoms leaving epitaxial sites and becoming more highly coordinated. This in contrast to the EAM, where Cu preferred to stay on epitaxial sites. However, as the *k*-point sampling was increased or more layers were added to the slab in the DFT studies, the Cu tended to move back to epitaxial positions. While we were not able to carry these calculations to full convergence, the trends suggest that the EAM and DFT agree on the geometries for larger-size Cu clusters on Ag.

III. TAD RESULTS

A. Film structure

As seen in previous experimental investigations[12,39,40] and conventional MD simulations,[41] the Cu film in the present study was pseudomorphic with the Ag substrate, taking on the Ag lattice parameter in the film plane. This 13% Bain distortion in the Cu deposit shrinks the out-of-plane lattice parameter, such that the Cu structure is body-centered tetragonal. After deposition of 1.5 ML of Cu in the present study, the average layer spacings were substrate-layer 1, 0.171 nm; layer 1-layer 2, 0.134 nm; layer 2-layer 3, 0.129 nm. Thus the spacings of the Cu layers were smaller than the body-centered-cubic spacing for the expanded lattice, which would be 0.145 nm. A molecular statics calculation for a Cu film of three full layers on (001)Ag, using the same EAM potential, gave these same three spacings as 0.176, 0.144, and 0.142 nm, which indicates the effect of island size on the layer spacings. Theoretical studies[42,43] have shown that the strained bct Cu structure is unstable, but it can be maintained for sufficiently thin films on a suitable substrate. No thermal mobility of deposited Cu atoms was observed in the TAD simulation until atoms were deposited into the second film layer. [No Cu jump or Cu-Ag exchange transitions on the (001)Ag surface were accepted]. These atoms were able to diffuse via exchange mechanisms with first-layer Cu atoms, as will be described in the following section. This diffusion allowed the formation of a compact island in the second film layer, as demonstrated in Fig. 1, which compares the film structure after 1.5-ML Cu deposition by the TAD simulation with that produced by conventional MD, which did not allow sufficient time for terrace diffusion. As noted in the previous section, the same initial locations for depositing Cu atoms were used in both simulations. The second film layer was approximately half filled in each simulation, but the TAD run

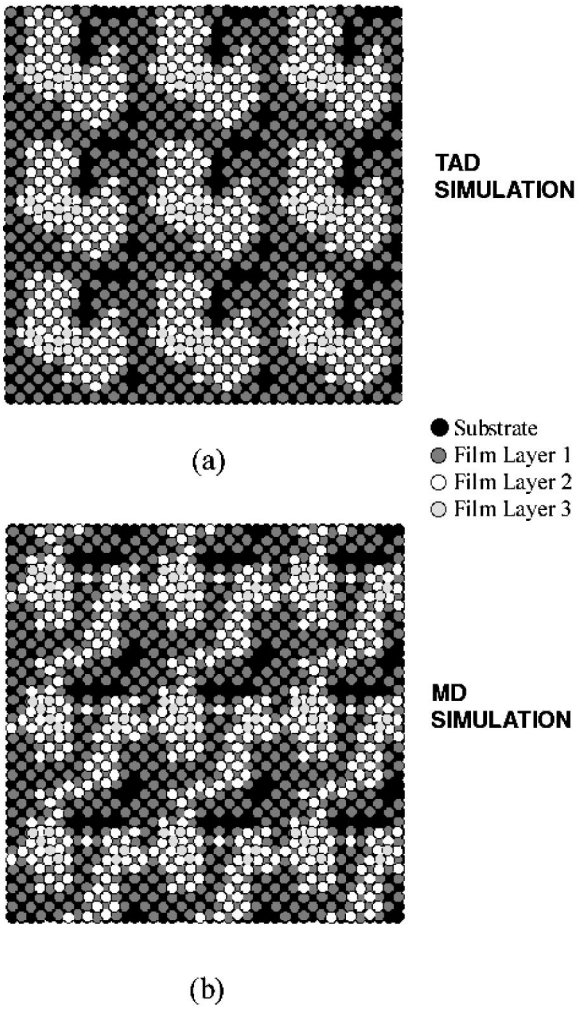

FIG. 1. Film layer structures following 1.5 ML of Cu deposited on (001)Ag at 77 K for (a) TAD simulation, average deposition rate 0.04 ML/s; (b) conventional MD simulation, deposition rate 5×10^{9} ML/s. To aid visualization of the structures, 3×3 expansions of the computational cell are shown.

produced a notably more compact second-layer island. To aid the visualization, 3×3 expansions of the simulation cells in the film plane are shown in the figure. As might be expected from the lack of thermal mobility observed for Cu atoms deposited directly on the Ag substrate, the first film layers from the two simulations were very similar. In both TAD and MD runs, the final films each had seven atoms in the third film layer, which were too few to allow any conclusions about morphological differences between these layer structures. Following steepest-descent relaxation, the potential energy of the TAD-simulated 1.5-ML (film+substrate) structure was 2.8-eV lower than the structure simulated by conventional MD.

Although Fig. 1 shows a qualitative effect of thermal diffusion on the second film layer structure at 77 K, the dependence of the number of atoms in this layer on the number of deposited atoms was virtually identical for the TAD and MD runs. To quantify the development of the compact island structure, a determination was made of the total number of nearest-neighbor pairs per atom within the second film layer

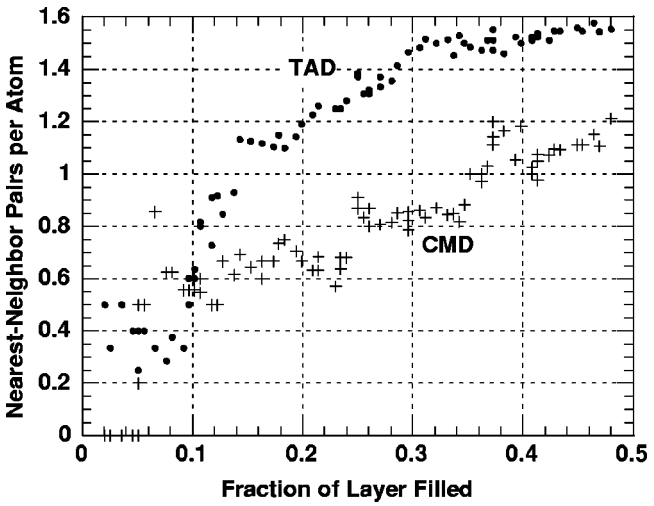

FIG. 2. Number of nearest-neighbor atom pairs in film layer 2 as a function of the fractional filling of that layer. The plots show Cu deposited on (001)Ag at 77 K as simulated by (a) TAD, average deposition rate of 0.04 ML/s; (b) conventional MD, deposition rate of 5×10^{9} ML/s.

after deposition of each Cu atom. This is shown in Fig. 2, which compares the conventional MD simulation with the TAD results as a function of the filling of the second film layer. The TAD simulation produced a maximum of about twice the number of nearest-neighbor pairs observed in the MD simulation at about 20% layer filling (1-ML total deposition). This ratio reduced to about 1.3 at about 50% layer filling. As a point of reference, both nearest-neighbor counts would obviously approach two per atom as this film layer filled completely.

B. Thermally activated processes

During the simulation of growth of 1.5 ML of Cu (147 atoms) on (001)Ag, a total of 2 215 572 thermally activated transitions were accepted at the system temperature of 77 K. The great majority of these transitions were multiple repetitions of low-barrier processes. If each distinct transition is only counted once, this number is reduced to 297, still an average of about two per deposited atom. The accepted transitions were selected from 4451 distinct activated processes observed during the basin-constrained MD simulations at 550 K. The accepted transitions can be conveniently divided into terrace-diffusion processes, which did not change the occupancies of the different film layers, and interlayer transport processes, which increased the occupancy of one film layer and decreased another. The details of some of these events will be presented in the following subsections.

1. Terrace-diffusion events

As noted above, all of the accepted terrace-diffusion transitions involved exchange between first- and second- or second- and third-layer Cu atoms. All of the events involving first- and second-layer atoms were transitions between two on-lattice configurations. However, the local environment of a terrace-diffusion event significantly affected its activation barrier and transition energy change (ΔE), as shown in Fig. 3. For example, the transitions of both Figs. 3(a) and 3(b) are exchange motions of a member of an isolated Cu trimer, but the barrier of the transition in Fig. 3(a) is higher by 0.06 eV. This energy difference is not large, but it does represent a ratio of reaction rates of greater than 8000 at 77 K (assuming similar prefactors). Also note that we are evaluating relative barriers of different atomic configurations, which should be more reliable than the absolute values of transition barriers for a given set of interatomic potentials. The Fig. 3(a) transition and its reverse occurred with similar rates in the TAD simulation, as expected from the similar end-state energies. The end-state energy difference of the Fig. 3(b) transition, however, gives its reverse reaction an exponential factor of 4×10^{-17} at 77 K, effectively preventing it from occurring. The transition of Fig. 3(c) involves another Cu trimer, which

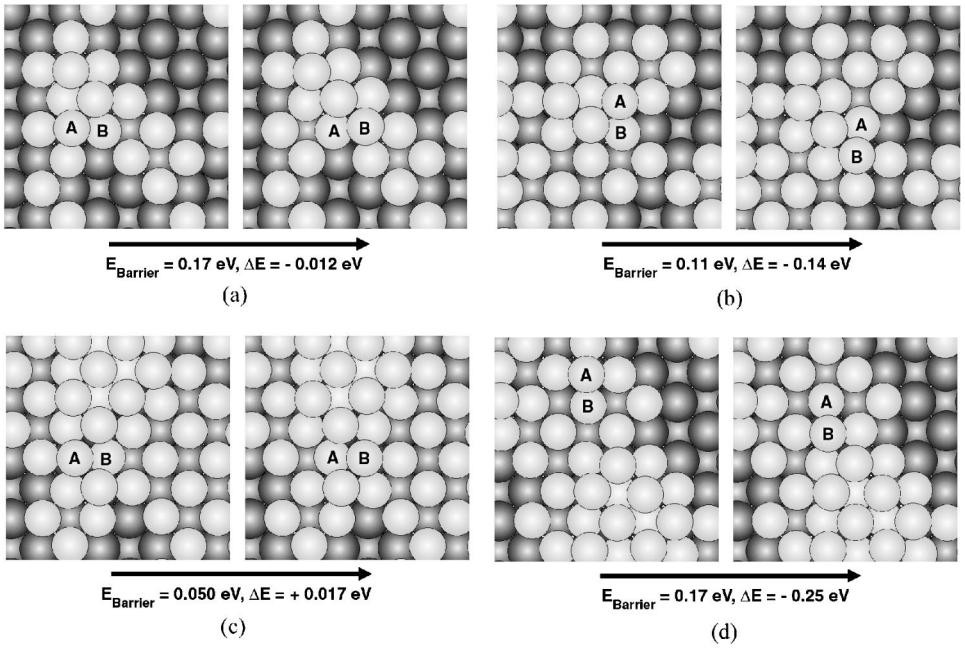

FIG. 3. Representative terrace-diffusion events observed for layer-2 Cu atoms: (a) and (b) motion of a member of an isolated trimer; (c) motion of a member of a trimer attached to larger cluster; (d) compacting transition of an isolated atom.

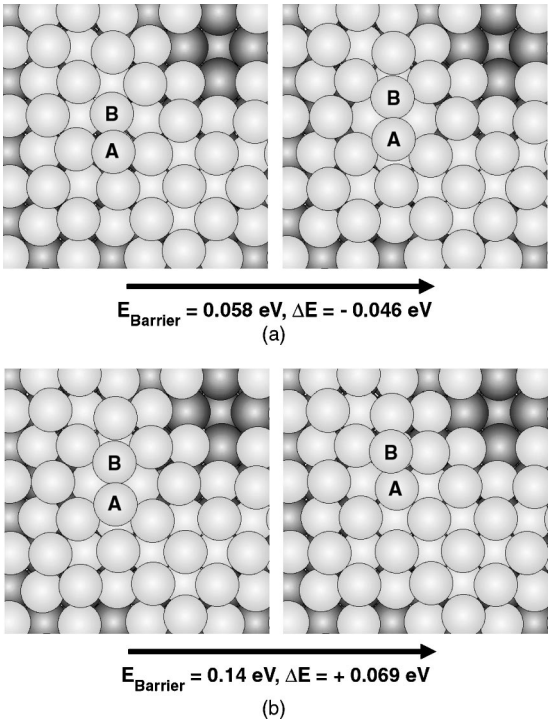

FIG. 4. Pair of terrace-diffusion events for layer-3 Cu atoms involving an off-lattice configuration: (a) on-lattice state 1 to off-lattice state; (b) off-lattice state to on-lattice state 2. Note that for this pair of transitions, the off-lattice configuration had the lowest potential energy of the three states.

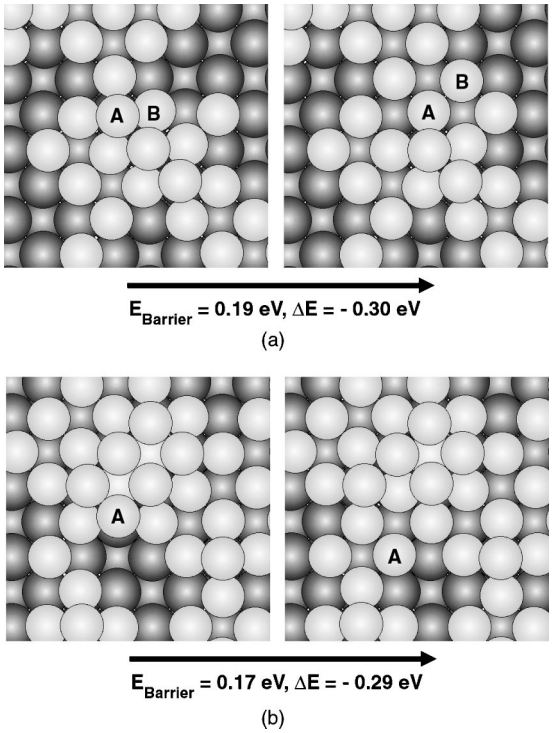

FIG. 5. Two interlayer transport events moving atoms from film layer 2 to film layer 1: (a) exchange event, assisted by existing layer-1 atoms; (b) over-the-edge transport from a fivefold coordinated layer-2 site to a sevenfold coordinated layer-1 site.

is attached to a larger cluster in the second film layer. The low activation barrier of this configuration gave this transition a waiting time of approximately 2 ps and caused this event and its reverse to occur a total of more than 500 000 times during 0.8 s of system time. Obviously, the analyses of these transitions would have effectively stopped the simulation without the KMC (synthetic mode) extension of TAD. The Fig. 3(d) transition is an example of the type of event that led to the compact island configuration seen in Fig. 1. The potential-energy difference between the two end states effectively stabilizes the compact structure. In general, transitions such as this gave decreases in potential energy of 0.15–0.30 eV.

Once atoms began to be deposited into the third film layer, an intermediate-energy minimum appeared along the exchange diffusion path for many transitions. This intermediate, off-lattice state could be either higher or lower in energy than the adjoining on-lattice states. Figure 4 illustrates one such pair of transitions for which the off-lattice configuration was more stable than either of the on-lattice states, albeit by small energy differences. Series of such transitions were seen to occur until either an atom was transferred from the third to the second layer, as discussed below, or additional Cu atoms were deposited nearby, resulting in a stable third-layer island nucleus. All of these observed stable configurations had on-lattice atom positions.

2. Interlayer transport events

The other class of observed transitions in this system was the transport of atoms between adjacent film layers. The events involving layers 1 and 2 were all the transport of atoms from layer 2 to layer 1 by either atom exchanges or over-the-edge jumps. Two examples of these reactions are illustrated in Fig. 5. In Fig. 5(a), an atom in the second film layer displaces an atom at the edge of the first layer, moving it outward between two other first-layer atoms. All observed cases of this exchange descent mechanism involved filling in a vacant layer-1 site with at least two existing nearest-neighbor atoms in that layer. This is similar to the enhanced layer-filling mechanisms discussed by Trushin *et al.*,[44] and Montalenti and Voter[11] for homoepitaxial systems. The step-descent mechanism of Fig. 5(b) involved the motion over a ⟨100⟩-type edge from a fivefold coordinated site (all Cu-Cu) to a sevenfold coordinated site (four Cu-Ag and three Cu-Cu).

The processes involving net transport between layers 2 and 3 were more complex. Both directions of net atom transport were observed, although movement from layer 3 to layer 2 was more common. Many observed events involved atoms in all three film layers. Figure 6 shows two such events. The mechanism illustrated in Fig. 6(a) involved a concerted three-atom movement: layer 3 to layer 2, layer 2 to layer 1, and layer 1 to layer 2. Similar processes were observed several times during the TAD run and were the primary mechanisms by which atoms deposited into film layer 3 were transported to lower terraces, although over-the-edge jumps were observed for atoms deposited into sites at the edge of a layer-2 terrace. Figure 6(b) shows an event that produced a net movement of one atom from film layer 2 to film layer 3. The layer motions in this event were effectively

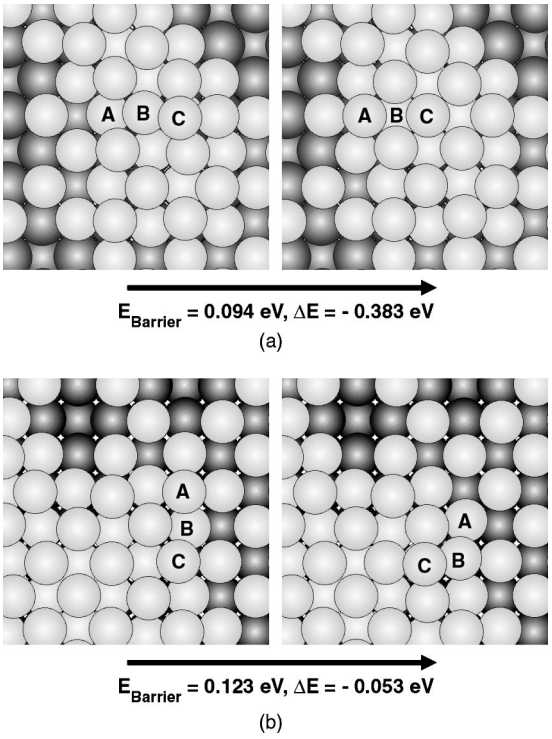

FIG. 6. Three-layer diffusion events: (a) net movement of one atom from layer 3 to layer 2; (b) net movement of one atom from layer 2 to layer 3.

the inverse of the Fig. 6(a) event, except that the movements were not all in the same lateral directions.

IV. DISCUSSION

A. Film structure

Comparing the results of the TAD simulation and the conventional MD simulation in either Figs. 1 or 2, we can see that the short-range thermal atomic mobility included in the TAD simulation due to its lower deposition rate (approximately a factor of 10^{11}) significantly affected the film morphology. The TAD simulation produced one fairly compact island in the computational cell, while the MD simulation resulted in a more random structure. Previous work of Bartelt and Evans[45] described the temperature dependence of homoepitaxial Ag(001) growth as comprising a low-temperature self-affine regime below approximately 130 K and a mounding regime at higher temperatures. In the self-affine regime, film roughness decreased with increasing temperature due to downward funneling reactions in the absence of significant terrace diffusion. In the mounding regime, film roughness increased with increasing temperature due to a combination of terrace diffusion and the Ehrlich-Schwoebel barrier to interlayer atomic transport. Because only 1.5 ML of Cu was deposited on a relatively small substrate in the present TAD simulation, we cannot directly compare our results with those of Bartelt and Evans, but the TAD results do imply that there is a low-temperature regime for Cu growth on (001)Ag in which a combination of short-range terrace diffusion and the lack of a significant Ehrlich-Schwoebel barrier produce small compact flat film terraces. A number of results in the literature have indicated that a RHEED experiment, such as that of Egelhoff, Jr. and Jacob,[12] does not provide sufficient evidence to prove the existence of such compact film islands. However, it should be possible to use a variable-temperature scanning-tunneling microscope (STM) with low-rate deposition capability to directly observe these structures. Limitations of the semiempirical EAM potential used in the present study might shift the exact onset temperature for the predicted terrace mobility, but the predicted effect of pseudomorphic film strain on the atomic transport should still be valid.

The TAD-simulated film structures in this investigation are consistent with the observations of Hahn *et al.*[46] for Cu deposited on (001)Pd at 300 K, even considering that these results were obtained on a heteroepitaxial system with less biaxial tensile film strain. They observed the nucleation of a high density of irregular Cu islands on the Pd substrate, which grew two-dimensionally to form a complete single layer for 1 ML of deposition. A much lower density of islands nucleated in the second layer. These were rectangular with ⟨110⟩ edges and also grew two dimensionally. They observed a spacing of the first layer from the substrate of 0.19 nm, with 0.155 nm between the first and second layers. The Hahn *et al.* interpretation of these results was that the first layer was growing with the fcc structure, and that subsequent layers were growing as a metastable body-centered-tetragonal phase with reduced strain, as evidenced by the smooth ⟨110⟩ edges of the islands. This interpretation was questioned by Alippi, Marcus, and Sheffler,[42] who showed that the bct Cu structure should be inherently unstable. The present TAD simulation provides further support for this latter view. The higher density of islands nucleated in the first film layer would be expected from the higher surface diffusion barrier for Cu atoms in this layer. For the case of Cu on (001)Ag, the barriers were 0.62 eV for first-layer atoms vs less than 0.2 eV for second-layer atoms. The larger layer spacing between the substrate and the first film layer is simply a reflection of differences between Cu-Ag or Cu-Pd and Cu-Cu interaction potentials. The two-dimensional growth of islands is due to relatively low barriers for interlayer atom transport—note the 0.09–0.17-eV barriers shown in Figs. 5 and 6. Finally, the rectangular second-layer islands with ⟨110⟩ edges are consistent with the second-layer island formed in the TAD simulation [Fig. 1(a)], which was a constrained unstable structure, not a metastable one.

B. Observed transitions

The effects of strain in the pseudomorphic Cu film on the activation barriers of surface diffusion processes and the effects of local environment on these barriers are perhaps the most interesting results of the present TAD simulation. The general effect of film strain on surface diffusion barriers can be easily understood by some simple model calculations. For this purpose, a (001)Cu cell was set up with three fixed and three active layers. A single Cu adatom was placed on this surface, and the activation barriers for ⟨110⟩ hop and ⟨100⟩ exchange diffusion of the adatom were calculated as a func-

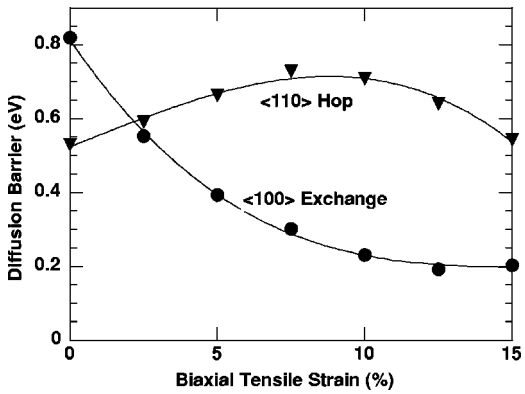

FIG. 7. Effect of biaxial tensile strain on the ⟨110⟩ hop and ⟨100⟩ exchange surface diffusion reactions on (001) Cu. System is a single Cu adatom on a (001)Cu substrate comprising three active and three fixed layers. The substrate is biaxially strained in the plane of the substrate. Lines are shown simply to guide the eye.

tion of imposed biaxial tensile strain in the underlying Cu. These results are shown in Fig. 7. With increasing tensile strain, the hop barrier increased from 0.53 to 0.73 eV at 7.5% strain and decreased back to 0.54 eV at 15% strain. The exchange barrier was 0.82 eV at zero strain, but decreased to less than 0.23 eV for strains greater than 10%. Also, the exchange barrier had a shallow secondary minimum for off-lattice atomic positions at strains greater than 10%. These calculations imply that the strain-enhanced atom mobility seen for Cu deposited on (001)Ag could also occur for Cu deposited on Pd, Pt, or Au. In this regard, pseudomorphic strained thin films of Cu have been observed for vapor deposition on (001)Pd,[46] as discussed above, and electrodeposition on (001)Au[47] and Ag,[48] although these experiments were all carried out at ambient temperature and above.

The effect of film strain on the interlayer transport mechanisms was even more dramatic. To illustrate this fact, a somewhat different approach was used. The initial atomic configuration of Fig. 6(a) was used as the starting point. For this configuration, the identity of all substrate atoms was changed to Cu, the computational cell was scaled to the equilibrium Cu lattice parameter, and the system was relaxed to minimum-energy atomic positions. The activation barrier of the Fig. 6(a) transition was then determined by the nudged-elastic-band method. This gave a transition barrier of 1.04 eV, more than a factor-of-10 greater than that for the strained Cu lattice.

Note that the transport mechanisms that were activated at 77 K in this study are specific to a strained heteroepitaxial film/substrate system. These phenomena are distinct from the reentrant layer-by-layer growth reported by Kunkel *et al.*,[49] for Pt deposited on (111)Pt. In that work, they reported smooth layer-by-layer growth at high temperature (621 K), rough three-dimensional growth at intermediate temperature (424 K), and relatively smooth quasi-layer-by-layer growth at low temperature (275 K). Their interpretation, now generally accepted, was that transport between film layers was efficient at the high temperature, but was inhibited at the intermediate temperature. At the low temperature, interlayer transport again becomes active, due to small island sizes and irregular island shapes. It would be interesting to investigate whether this reentrant layer-by-layer growth phenomenon would also occur for a strained heteroepitaxial system such as Cu on (001)Ag. At present, however, TAD simulations of film growth at experimental deposition rates are limited to system temperatures below about 100 K, due to the decrease in available boost with increasing system temperature. A detailed discussion of this point can be found in the literature.[50] Further developments of the TAD method are being pursued to reduce this limitation, so that such a study may become feasible in the future.

Even though this TAD simulation involved the deposition of only 1.5 ML of Cu, it is interesting to consider whether any of the observed mechanisms, especially the stabilization of off-lattice atomic configurations, could affect the increasing instability of the strained pseudomorphic Cu films with increasing film thickness. The limited TAD results for layer-3 atoms tend to argue against this possibility. As more than a few Cu atoms agglomerated in the third film layer, the on-lattice configurations appeared to become stabilized. This conclusion would be consistent with the STM observations of Cu electrodeposited on (001)Ag (Ref. 48) and (001)Au (Ref. 47) and synchrotron x-ray scattering observations of Cu electrodeposited on (001)Au,[51] which all found that the Cu films grew pseudomorphically to about 10 ML, after which the films restructured by buckling reactions.

The activation barriers of the 4451 events recorded (including those not accepted) during basin-constrained MD simulations at 550 K are shown in Fig. 8(a). In general, the distribution can be described as a tail of low-barrier transitions below 0.1 eV with the major distribution spanning 0.1–0.5 eV. The high-energy decrease in the number of observed transitions easily can be seen to result from the waiting times for these transitions. The distribution of waiting times before a transition for our assumed first-order statistics is given by

$$P(t>\tau)=\exp(-\text{rate}*\tau), \tag{6}$$

where $P(t>\tau)$ is the probability that a possible transition will have a waiting time greater than τ, and the rate is given by Eq. (1). For the conditions of the present TAD simulation, Eq. (3) defines the average simulation time at the elevated temperature between atom depositions as approximately 1.5×10^{-10} s. If we assume a rate prefactor of 3×10^{12} per s, Eqs. (3) and (1) predict that a transition with an activation barrier of 0.5 eV will have a 99% probability of having a waiting time beyond the next deposition.

The activation barrier distribution of the 297 unique accepted transitions at the 77-K system temperature is given in Fig. 8(b). As one would expect, the tail of low-barrier transitions also appears in this distribution, but it is much more prominent, due to the much smaller number of higher-barrier events. This activation energy distribution suggests that 77 K is close to the threshold temperature for significant atom mobility in this system. The transition rate of a reaction with a barrier of 0.15 eV would be a factor-of-approximately-30 lower at 67 than at 77 K. It is also interesting to note that the 0.09–0.18-eV spread of observed activation barriers repre-

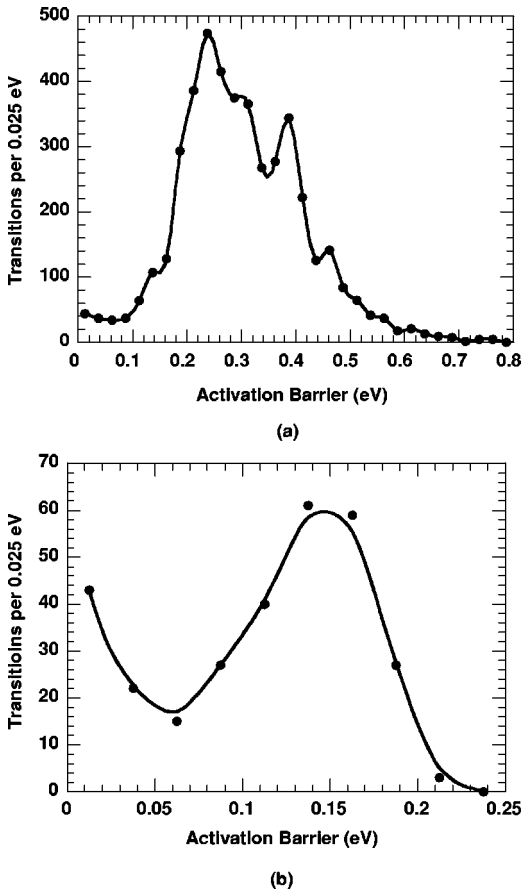

FIG. 8. Distributions of activation barriers for events in the TAD simulation of growth of 1.5 ML of Cu on (001) Ag: (a) events observed at the elevated temperature of 550 K; (b) events accepted at the system temperature of 77 K. In each case, repetitions of identical events are counted only once. Lines are smooth curves shown simply to guide the eye.

sents approximately a ratio of 8×10^5 in reaction rates (not allowing for differences in rate prefactors) at the system temperature of 77 K. In contrast, the same range of activation barriers represents a factor of less than 7 at the elevated temperature of 550 K. This illustrates the need for the TAD analysis to correctly calculate system dynamics from a temperature-accelerated simulation.

V. SUMMARY AND CONCLUSIONS

Temperature-accelerated dynamics (TAD) simulation using embedded-atom method (EAM) potentials has been applied to study the growth of a Cu film on Ag(001) at a temperature of 77 K and a deposition rate of 0.04 ML/s. The Cu grew as a biaxially strained pseudomorphic film with a body-centered-tetragonal structure. The biaxial tensile strain in the Cu film lowered the transition barriers for several surface exchange diffusion mechanisms involving atoms in the second and higher film layers, which caused them to occur at significant rates at 77 K. These diffusion processes produced compaction of Cu islands and a significantly different film microstructure from that produced in a conventional molecular-dynamics (MD) simulation of the same deposition. The local atomic environment sufficiently affected the activation barriers to cause large variations in reaction rates for otherwise similar processes. These variations would make it very difficult to simulate this system by a kinetic Monte Carlo method that requires *a priori* knowledge of the kinetics for all atomic processes.

ACKNOWLEDGMENTS

J.A.S. was supported by the Office of Naval Research. He also gratefully acknowledges the facilities provided by the U.S. Department of Energy during his sabbatical at Los Alamos National Laboratory. The work at Los Alamos National Laboratory was carried out under the auspices of the U.S. DOE (Contract No. W-7405-ENG-36). A.F.V. was supported by the Office of Science/Office of Basic Energy Sciences/ Division of Materials Science. B.P.U. acknowledges funding from a cooperative research and development agreement (CRADA) with Motorola Corporation. The work of Mads Sørensen in writing the TAD computer code is also gratefully acknowledged.

[1] K.-H. Müller, Phys. Rev. B **35**, 7906 (1987).
[2] Y. Yue, Y. K. Ho, and Z. Y. Pan, Phys. Rev. B **57**, 6685 (1998).
[3] J. W. Evans, D. E. Sanders, P. A. Thiel, and A. E. DePristo, Phys. Rev. B **41**, 5410 (1990).
[4] F. Montalenti and A. F. Voter, Phys. Rev. B **64**, 081401(R) (2001).
[5] J. A. Sprague and C. M. Gilmore, Thin Solid Films **272**, 244 (1996).
[6] M. C. Bartelt and J. W. Evans, Surf. Sci. **423**, 189 (1999).
[7] A. F. Voter, Phys. Rev. B **34**, 6819 (1986).
[8] M. R. Sørensen and A. F. Voter, J. Chem. Phys. **112**, 9599 (2000).
[9] A. F. Voter, F. Montalenti, and T. C. Germann, Annu. Rev. Mater. Res. **32**, 321 (2002).
[10] F. Montalenti, M. R. Sørensen, and A. F. Voter, Phys. Rev. Lett. **87**, 126101 (2001).
[11] F. Montalenti and A. F. Voter, Phys. Status Solidi B **226**, 21 (2001).
[12] W. F. Egelhoff, Jr. and I. Jacob, Phys. Rev. Lett. **62**, 921 (1989).
[13] J. W. Evans, Phys. Rev. B **43**, 3897 (1991).
[14] H.-N. Yang, G.-C. Wang, and T.-M. Lu, Phys. Rev. B **51**, 17 932 (1995).
[15] M. I. Haftel, M. Rosen, T. Franklin, and M. Hettermann, Phys. Rev. B **53**, 8007 (1996).
[16] G. H. Vineyard, J. Phys. Chem. Solids **3**, 121 (1957).
[17] C. H. Bennett, in *Algorithms for Chemical Computations*, edited by R. E. Christofferson (American Chemical Society, Washington, DC, 1977).
[18] D. Chandler, J. Chem. Phys. **68**, 2959 (1978).
[19] J. B. Anderson, Adv. Chem. Phys. **91**, 381 (1995).

[20] H. Jónsson, G. Mills, and K. W. Jacobsen, in *Classical and Quantum Dynamics in Condensed Phase Simulations*, edited by B. J. Berne, G. Ciccotti, and D. F. Coker (World Scientific, Singapore, 1998).
[21] G. Henkelman and H. Jónsson, J. Chem. Phys. **113**, 9978 (2000).
[22] M. S. Daw and M. I. Baskes, Phys. Rev. B **29**, 6443 (1984).
[23] A. F. Voter and S. P. Chen, Mater. Res. Soc. Symp. Proc. **82**, 175 (1987).
[24] A. F. Voter, in *Intermetallic Compounds: Principles and Practice*, edited by J. H. Westbrook and R. L. Fleischer (Wiley, New York, 1994), Vol. 1, p. 77.
[25] A. F. Voter, Los Alamos Unclassified Technical Report No. LA-UR-93-3901, 1993 (unpublished).
[26] A. F. Voter, Phys. Rev. B **57**, 13 985 (1998).
[27] A. F. Voter, Proc. SPIE **821**, 214 (1987).
[28] R. A. Johnson, Phys. Rev. B **39**, 12 554 (1989).
[29] S. M. Foiles, M. I. Baskes, and M. S. Daw, Phys. Rev. B **33**, 7983 (1986).
[30] C. L. Liu, J. M. Cohen, J. B. Adams, and A. F. Voter, Surf. Sci. **253**, 334 (1991).
[31] G. Boisvert and L. J. Lewis, Phys. Rev. B **56**, 7643 (1997).
[32] B. D. Yu and M. Scheffler, Phys. Rev. B **55**, 13 916 (1997).
[33] F. Montalenti and R. Ferrando, Phys. Rev. B **59**, 5881 (1999).
[34] G. Kresse and J. Hafner, Phys. Rev. B **47**, 558 (1993).
[35] D. Vanderbilt, Phys. Rev. B **41**, 7892 (1990); G. Kresse and J. Hafner, J. Phys.: Condens. Matter **6**, 8245 (1994).
[36] Y. Wang and J. P. Perdew, Phys. Rev. B **44**, 13 298 (1991).
[37] G. Henkelman, B. P. Uberuaga, and H. Jónsson, J. Chem. Phys. **113**, 9901 (2000).
[38] In this work, we are not attempting to report fully converged *ab initio* results. Our goal was simply to take the largest simulation cell we could afford to consider (73 atoms), together with the maximum number of k points ($2\times2\times1$), and make a comparison between *ab initio* and EAM activation energies. Still, from the results we obtained, it appears that the jump and exchange barriers reported in this paper are already sufficiently converged with our simulation parameters.
[39] Z. Q. Wang, S. H. Lu, Y. S. Li, F. Jona, and P. M. Marcus, Phys. Rev. B **35**, 9322 (1987).
[40] H. Li, D. Tian, J. Quinn, Y. S. Li, F. Jona, and P. M. Marcus, Phys. Rev. B **43**, 6342 (1991).
[41] J. A. Sprague and C. M. Gilmore, in *Materials Modification by Energetic Atoms and Ions*, edited by K. S. Grabowski, S. A. Barnett, S. M. Rossnagel, and K. Wasa, Mater. Res. Soc. Symp. Proc. Proceedings No. 268, 115 (Materials Research Society, Pittsburgh, 1992).
[42] P. Alippi, P. M. Marcus, and M. Scheffler, Phys. Rev. Lett. **78**, 3892 (1997).
[43] Y. Mishin, M. J. Mehl, D. A. Papaconstantopoulos, A. F. Voter, and J. D. Kress, Phys. Rev. B **63**, 224106 (2001).
[44] O. S. Trushin, K. Kokko, P. T. Salo, W. Hegert, and M. Kotrla, Phys. Rev. B **56**, 12 135 (1997).
[45] M. C. Bartelt and J. W. Evans, Phys. Rev. Lett. **75**, 4250 (1995).
[46] E. Hahn, E. Kampshoff, N. Wälchli, and K. Kern, Phys. Rev. Lett. **74**, 1803 (1995).
[47] R. Randler, M. Dietterle, and D. M. Kolb, Z. Phys. Chem. (Munich) **208**, 43 (1999).
[48] M. Dietterle, T. Will, and D. M. Kolb, Surf. Sci. **396**, 189 (1998).
[49] R. Kunkel, B. Poelsema, L. K. Verheij, and G. Comsa, Phys. Rev. Lett. **65**, 733 (1990).
[50] F. Montalenti and A. F. Voter, J. Chem. Phys. **116**, 4819 (2002).
[51] B. M. Ocko, I. K. Robinson, M. Weinert, R. J. Randler, and D. M. Kolb, Phys. Rev. Lett. **83**, 780 (1999).